Indonesian Physical Review

Volume 5 Issue 3, September 2022

P-ISSN: 2615-1278, E-ISSN: 2614-7904

The Structure Study of Nickel Doped Zinc Oxide Nanoparticles Synthesized by Coprecipitation Method

Destalina[1*], Fitriah Mujtahid[1], Inayatul Mutmainna[1], Dahlang Tahir[1], Paulus L Gareso[1*]

[1] *Physics department, Faculty Mathematics and Natural Science Hasanuddin University, Indonesia*

Corresponding Authors E-mail: destalina96@gmail.com, pgareso@fmipa.unhas.ac.id

Article Info

Article info:

Received: 07-07-2022

Revised: 24-07-2022

Accepted: 18-08-2022

Keywords:

X-ray Diffraction; Ni-doped ZnO; Coprecipitation

How To Cite:

Destalina, F. Mujtahid., I. Mutmainna., D. Tahir., P., L., Gareso. "XRD Stucture Study on Nickel Doped Zinc Oxide Nanoparticles Synthesized by Coprecipitation Method", Indonesian Physical Review, vol. 5, no. 3, p, 188-196, 2022.

DOI:

https://doi.org/10.29303/ipr.v5i3.179

Abstract

Nickel-doped Zinc Oxide ($Zn_{(1-x)}Ni_{(x)}O$) nanoparticles have been synthesized by the chemical coprecipitation method. The structure and characteristic of synthesized Ni doped ZnO nanoparticles ware analyzed by X-ray diffraction (XRD) patterns. Crystallite sizes and lattice strain of all samples were calculated using the Scherrer's formula, Uniform Deformation Model (UDM) and Halder-Wagner (H-W) method. X-ray diffraction analysis confirmed hexagonal cubic structure of Ni-doped ZnO nanoparticles. Also, the crystallite size of the nanoparticles reduces as the nickel concentration increase. The result showed the average crystallite size calculated by Scherrer's formula (25-29 nm) was smaller than crystallite size using UDM method (51-63) the largest average crystallite size and H-W method (42-47 nm). The lattice strain increases with decreasing crystallite sizes value. The crystal size Ni- doped ZnO nanoparticles decreased with increasing dopant concentration.

Introduction

Semiconductor nanoparticles have unique characteristics[1]. The study of zinc oxide (ZnO), a multi-functional metal oxide semiconductor material with a direct wide band gap (3.37 eV), which has a wurtzite crystal structure and has attracted interest in the last decade. The investigation of the change in properties arising from doping different transition metals such as Co, Mn, Fe, Ni, and Cr to ZnO has become a popular research subject[2][3][4]. One of the materials used as doping is Nickel (Ni). The used nickel in this study increases the

electrical conductivity of ZnO. Ni has good optical and electrical properties due to low oxygen reactivity[5].

Many methods were used to synthesize ZnO nanoparticles such as the sol-gel [6], coprecipitation [7][8], hydrothermal, chemical bath deposition, and electrochemical deposition [9]. Among these various methods, the coprecipitation method has a high potential and is an economical, simple, and efficient deposition technique [10]. The coprecipitation method involves metal deposition with the assistance of an acid and base pair to regulate the nucleation and growth of particles. The metal precipitated is a hydroxide, carbonate, oxalate, or citrate. The metal precipitate formed is then calcined at a high temperature to obtain a mixture of oxides according to the desired target [11][12]. Synthesizing nickel-doped ZnO nanoparticles with the coprecipitation method which is an increased magnetization due to the decrease in particle size or crystallite size due to the nickel clustering [13]. Coprecipitation method play a major role in defining the magnetic ordering[14].

In this study, Ni-doped ZnO nanoparticles were synthesized using the coprecipitation method with various concentration ratios of nickel 0 to 11%. The structure and characteristics of the Ni-doped ZnO nanoparticles were analyzed using X-ray diffraction using Scherrer formula, Williamson-Hall (UDM) and Halder Wagner method.

Experimental Method

All precursor materials are of high purity analytical grade. Zinc acetate dihydrate ($Zn(CH_3COO)_2.2H_2O$), nickel hexahydrate ($Ni(NO_3)_2.6H_2O$), sodium hydroxide (NaOH) and deionized water (99,998%). Synthesis of the Ni-doped ZnO samples ($Zn_{(1-x)}Ni_{(x)}O$ where x = 0.05, 0.06, 0.07, 0.09 and 0.11) were prepared by coprecipitation method. Zinc acetate dihydrate ($Zn(CH_3COO)_2.2H_2O$) and nickel hexahydrate ($Ni(NO_3)_2.6H_2O$) were dissolved in 150 ml deionized water and NaOH (0.5 M) solution was added to the precursor solution until the pH value had reached 8. The combination was magnetically stirred continuously at 85°C for 2h. The precipitate was separated from the solution by filtration, washed several times with deionized water. Then calcined at 550°C for 3 hours [12][15].

The crystalline structure and the crystalline size of the prepare Ni- doped ZnO nanoparticles analyzed using X-ray diffractometer.

Result and Discussion

The diffraction pattern of $Zn_{1-x}Ni_xO$ (x = 0.05, 0.06, 0.07, 0.09 and 0.11) shown in Figure 1, using Cu Kα radiation. The diffraction peaks have cubic and hexagonal structures for samples with various variations corresponding to the standard peaks of ZnO (JCPDS Card No: 01-079-0206). With the peak value (hkl) obtained, namely (100), (002), (101), (102), (110), (103), (112), (200) and (201). These reflection planes of the (hkl) are correlated to the diffraction angle of 2θ: 31.77º, 34.42º, 36.25º, 47.54º, 56.59º, 62.86º, 66.37º, 67.95º, and 69.08º.

The synthesized ZnO nanoparticle samples showed a substantial diffraction peak value at hkl (101), indicating the presence of a high percentage of the crystalline phase. Besides, there is no impurity phase in the sample [16]. The diffraction peak shift towards a lower value of 2θ, as shown in Figure 1(b), occurs with increasing Ni doping [17]. The lower angular shift in

the diffraction peak of Ni-doped ZnO sample is mainly due to the doping of the substituted Ni ion and distortion in the ZnO lattice[11]. The difference in the radius of the Ni^{2+} ion can be substituted at the Zn^{2+} position in the ZnO lattice[12][18]. In addition, the peak shift that occurred in all doped samples was also observed. Referring to the Bragg scattering law, the greater the scattering angle, the smaller the distance between the fields, and vice versa. The addition of Ni doping causes a shift to the right, where the scattering angle is getting bigger so that the distance between the planes is smaller. The stress in the ZnO lattice is caused by the distance between the planes. Nickel doping on ZnO nanoparticles causes a shift to the left so that the distance between the fields widens. This is influenced by the difference in ion radii and coordination number between Ni and Zn ions[19][20].

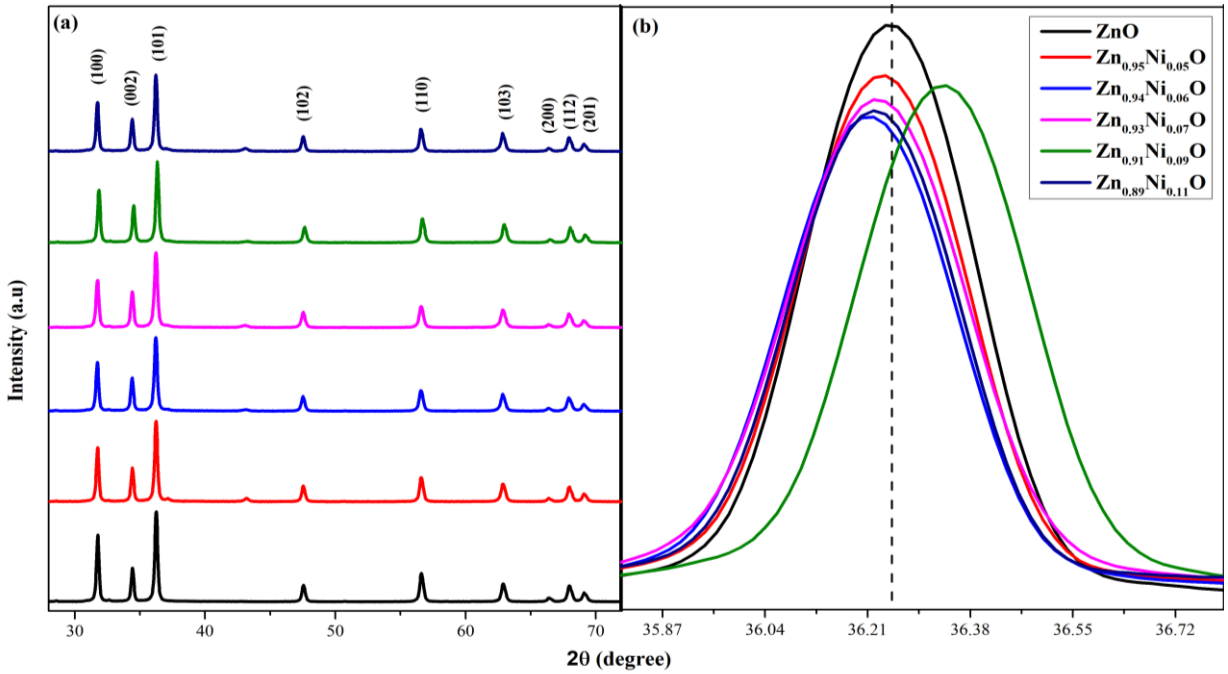

Figure 1. (a) XRD diffraction pattern of ZnO nanoparticles with Ni ion doping variation. (b) Peak shift in hkl (101).

Crystal size Ni-doped ZnO sample was analyzed using the Debye-Scherrer equation [11][21].

$$D = \frac{0.9\lambda}{\beta cos\theta} \quad (1)$$

The Bragg angle is expressed by θ, λ is the wavelength of X-ray radiation (1,54 Å), and β is the full width at half peak maximum (FWHM). The crystal sizes obtained from the addition $Zn_{0.95}Ni_{0.05}O$, $Zn_{0.94}Ni_{0.06}O$, $Zn_{0.93}Ni_{0.07}O$, $Zn_{0.91}Ni_{0.09}O$, and $Zn_{0.89}Ni_{0.11}O$ were 28.59 nm, 27.38 nm, 25.58 nm, 27.92 nm and 28.94 nm, and each showed a decrease in the crystal size of pure ZnO measuring 29.22 nm. The equation (1) shows an inverse relationship between β and D which means that narrower peaks are produced due to larger particles while wider peaks are obtained due to smaller particles[16]. Microstrain (ε) in the sample of Ni-doped ZnO nanoparticles was calculated using the equation;

$$\varepsilon = \frac{\beta cos\theta}{4} \quad (2)$$

The microstrain value obtained is inversely proportional to the crystal size value. The smallest strain was obtained in the sample $Zn_{0.89}Ni_{0.11}O$, and the largest in the sample $Zn_{0.95}Ni_{0.05}O$.

The crystal size and lattice strain of the ZnO sample with the variation of Ni doping were calculated using the Williamson-Hall equation representing the uniform deformation model (UDM). Where UDM, throughout the crystallographic direction, crystal imperfections and considers strain is isotropic[1].

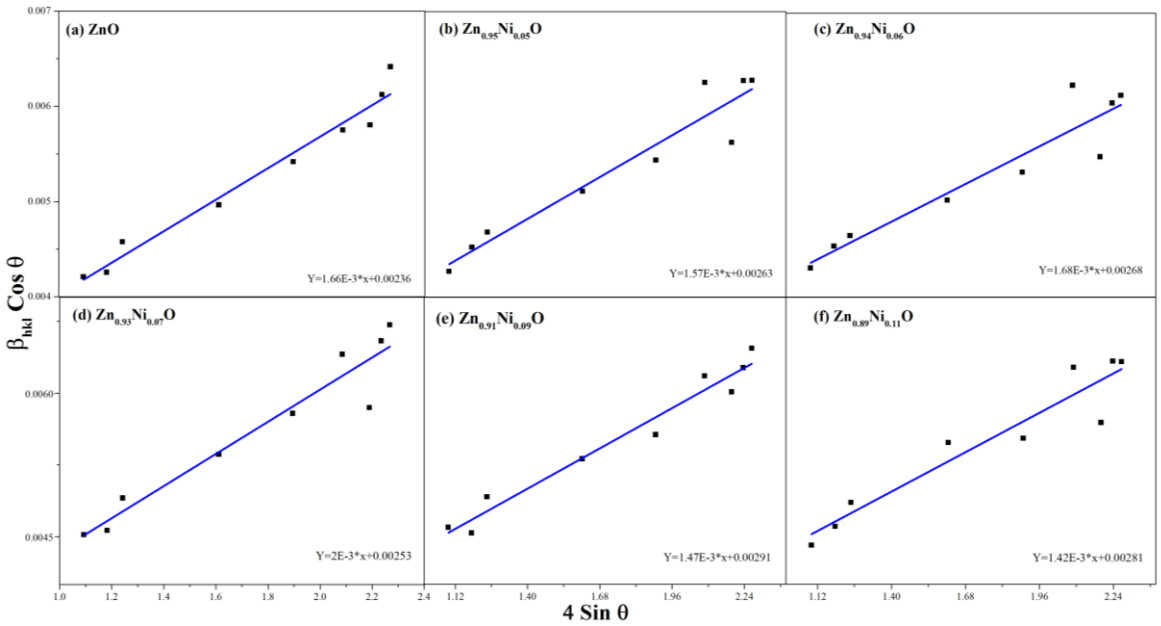

Figure 2. Williamson-Hall (UDM) plot for ZnO sample with Ni doping variation.

The peak broadening to strain can be expressed as[22];

$$\varepsilon = \frac{\beta_s}{4tan\theta} \quad (3)$$

$$\beta_{hkl} = \beta_s + \beta_D \quad (4)$$

$$\beta_{hkl}cos\theta = \frac{k\lambda}{D} + 4\varepsilon sin\theta \quad (5)$$

Diffraction angle(2θ); (β_{hkl}) is full width at half maximum (FWHM); (k) is the Scherrer constant, (λ) is the x-ray wavelength, (D) is the crystal size and (ε) is the lattice strain.

Lattice strain induces the observed peak widening of the diffraction pattern due to the presence of crystal defects and distortions. UDM representation where the x-axis is $4sin\theta$ and the y-axis is $\beta_{hkl}cos\theta$ shown in Figure 2. The intercept on the y-axis represents the crystal size (D), while the slope on the x-axis represents the lattice strain (ε)[23]. This strain is associated with the possible lattice shrinkage in the calculation of the lattice parameters[17]. The plot UDM's slope positive, which indicates the lattice expansion[24] and produces an intrinsic strain in the nanocrystals. Crystal size and intrinsic strain of the Ni-doped ZnO sample are shown in Table 1.

A better and more suitable widening of the isotropic line is given by the Halder-Wagner (H-W) method. In the Halder-Wagner method, peak widening is assumed to be a symmetrical Voigt function which is the convolution of the Lorentzian function and the Gaussian function in evaluating size and strain [21]. The FWHM approach with the Halder-Wagner method is given in the following equation

$$\beta_{hkl}^2 = \beta_L \beta_{hkl} + \beta_G^2 \quad (6)$$

where β_L is Lorentzian, FWHM and β_G are the Gaussian FWHM. Furthermore, the crystal size and lattice strain are expressed by the following equation:

$$\left(\frac{\beta_{hkl}^*}{d_{hkl}^*}\right)^2 = \frac{1}{D}\frac{\beta_{hkl}^*}{d_{hkl}^{*2}} + \left(\frac{\varepsilon}{2}\right)^2 \quad (7)$$

Where $\beta_{hkl}^* = \beta_{hkl}\, cos\theta/\lambda$ dan $d_{hkl}^* = 2\, sin\theta/\lambda$. Halder-Wagner plot representation is shown in figure 5 where $(\beta_{hkl}^*/d_{hkl}^{*2})$ is the x-axis and $(\beta_{hkl}^*/d_{hkl}^*)^2$ is the y-axis.

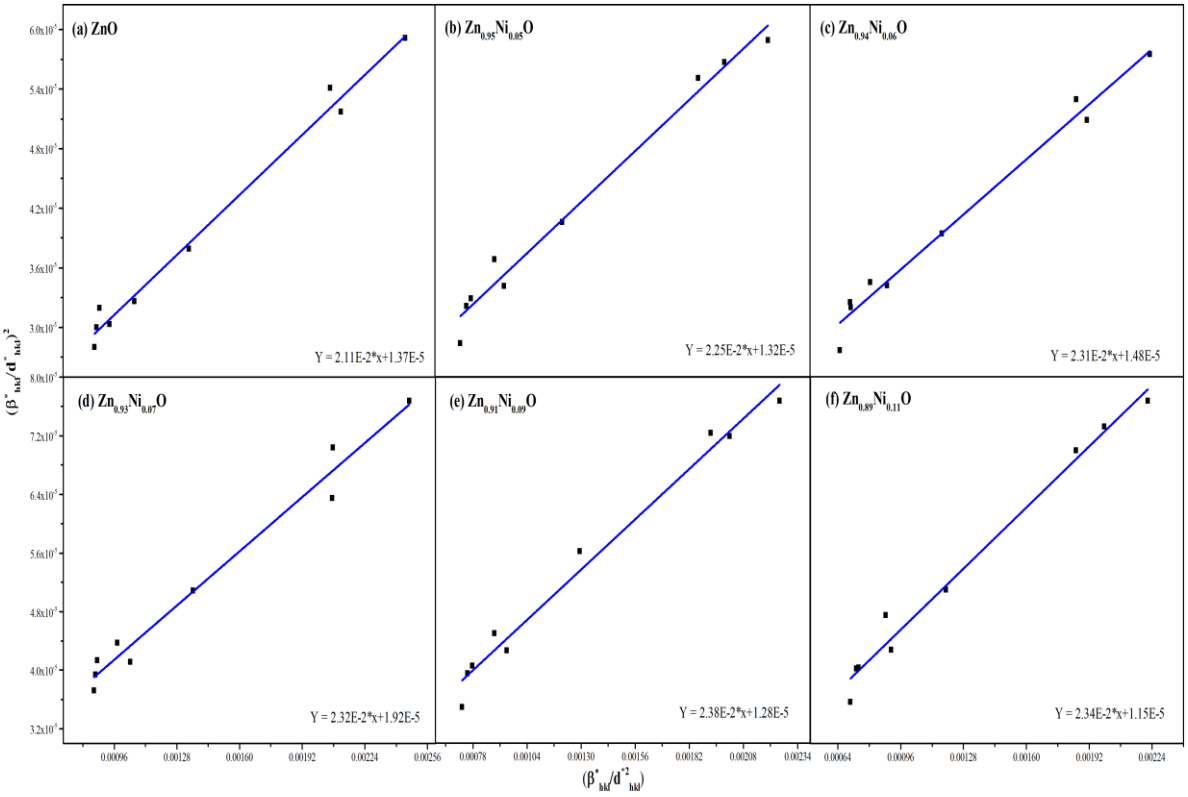

Figure 3. Halder-Wagner plot for ZnO sample with Ni doping variation.

Figure 3 shows the slope of the straight line indicates the average size of the crystal $Zn_{(0.95)}Ni_{(x)}O$. In contrast, the y-intercept shows the strain value. The crystallite size and the strain from Scherrer, UDM and H-W methods are shown in Table 1.

Table 1. The geometry parameters of the Ni-doped ZnO nanoparticles used different methods.

Sample	FWHM (deg)	Debye Scherrer	Williamson – Hall (UDM) method	Halder Wagner method

		D (nm)	ε *(10^{-3})	D (nm)	ε *(10^{-3})	D (nm)	ε *(10^{-3})
ZnO	0.344	29.22	3.11	63.95	1.66	47.42	14.79
$Zn_{0.95}Ni_{0.05}O$	0.351	28.59	3.18	57.38	1.57	44.50	14.54
$Zn_{0.94}Ni_{0.06}O$	0.367	27.38	3.33	56.31	1.68	43.19	15.40
$Zn_{0.93}Ni_{0.07}O$	0.394	25.58	3.56	59.65	2.00	43.27	17.54
$Zn_{0.91}Ni_{0.09}O$	0.358	27.92	3.25	51.86	1.47	42.02	14.34
$Zn_{0.89}Ni_{0.11}O$	0.345	28.94	3.14	53.71	1.42	42.69	13.55

The crystal size values of these three methods are slightly different. Determination of average crystallite size from Scherrer formula does not take into account the contribution of intrinsic strain which develops in a nanocrystal due the presence of point defect, stacking faults, grain boundaries, and it is not expected to be valid for very small crystallite sizes (<10 nm). Williamson–Hall (W–H) method is broadening of diffraction peaks is mainly due to crystallite size effects, microstrain and instrumental effects. The Halder-Wagner method is more accurate, with most of data points touching the fitting line compared with other methods. Therefore, one method is more accurate data points of (x,y) are more touching the fitting line [14].

In the UDM method, the crystal size ranges from 51-63 nm, slightly larger than the Scherrer and H-W method, which ranges from 25-29 nm to 42-47 nm. The crystal size of the three methods varied according to the doping variation. Lattice strain is inversely proportional to crystal size. The smaller the crystal size, the greater the strain value. The crystal size for the ZnO nanoparticle doped nickel samples decreased with increasing dopant concentration (0, 5, 6, 7, 9, and 11%) as shown in Table 1. This may be due to the distortion of the ZnO lattice by foreign impurities, and decreases the nucleation of Ni2+ and subsequent growth rate of the ZnO nanoparticles[11].

Conclusion

Ni-doped ZnO nanoparticles have been successfully synthesized using the coprecipitation method. X-ray diffraction analysis confirmed the cubic hexagonal ZnO structure and phase purity of all samples undisturbed by Ni-doped ZnO samples. Doping nickel concentration shifts the XRD peak of the hkl (101) plane to the hkl (002) plane in pure ZnO. The results were obtained for analyzing the peak profile of X-rays using the Scherrer equation, a modification of the UDM method and the Halder-Wagner method of strain size plot. It was found that the average particle size calculated by the Debye Scherrer equation (25-29 nm) is smaller than the particle size value using the Williams-Hall (UDM) method (51-63 nm) with the largest average particle size. While the mean size and strain size of the Halder-Wagner method (42-47 nm) are very suitable as observed in the study. Therefore, the widening of the XRD peaks by different methods showed the mean size distribution was in the range of 25–63 nm. The lattice strain is inversely proportional to the crystal size. The lattice strain increases with decreasing crystal size value. The crystal size for nickel samples doped with ZnO nanoparticles decreased with increasing dopant concentration.

References

[1] D. Nath, F. Singh, and R. Das, "X-ray diffraction analysis by Williamson-Hall, Halder-Wagner and size-strain plot methods of CdSe nanoparticles- a comparative study,"

Mater. Chem. Phys., vol. 239, no. August 2019, p. 122021, 2020, doi: 10.1016/j.matchemphys.2019.122021.

[2] P. Pascariu, I. V. Tudose, M. Suchea, E. Koudoumas, N. Fifere, and A. Airinei, "Preparation and characterization of Ni, Co doped ZnO nanoparticles for photocatalytic applications," *Appl. Surf. Sci.*, vol. 448, pp. 481–488, 2018, doi: 10.1016/j.apsusc.2018.04.124.

[3] Ş. Ş. Türkyılmaz, N. Güy, and M. Özacar, "Photocatalytic efficiencies of Ni, Mn, Fe and Ag doped ZnO nanostructures synthesized by hydrothermal method: The synergistic/antagonistic effect between ZnO and metals," *J. Photochem. Photobiol. A Chem.*, vol. 341, pp. 39–50, 2017, doi: 10.1016/j.jphotochem.2017.03.027.

[4] A. Noorhidayati, R. Philipus, M. P. Rachmawati, and R. Saleh, "Transition Metal (Ni, Cr)-Doped ZnO Assisted CTAB Performance on Decolorization of Organic Dyes," *Adv. Mater. Res.*, vol. 1123, no. 3, pp. 289–294, 2015, doi: 10.4028/www.scientific.net/amr.1123.289.

[5] S. Al-Ariki, N. A. A. Yahya, S. A. Al-A'nsi, M. H. H. Jumali, A. N. Jannah, and R. Abd-Shukor, "Synthesis and comparative study on the structural and optical properties of ZnO doped with Ni and Ag nanopowders fabricated by sol gel technique," *Sci. Rep.*, vol. 11, no. 1, pp. 1–11, 2021, doi: 10.1038/s41598-021-91439-1.

[6] M. F. Khan *et al.*, "Flower-shaped ZnO nanoparticles synthesized by a novel approach at near-room temperatures with antibacterial and antifungal properties," *Int. J. Nanomedicine*, vol. 9, no. 1, pp. 853–864, 2014, doi: 10.2147/IJN.S47351.

[7] R. Sagheer, M. Khalil, V. Abbas, Z. N. Kayani, U. Tariq, and F. Ashraf, "Effect of Mg doping on structural, morphological, optical and thermal properties of ZnO nanoparticles," *Optik (Stuttg).*, vol. 200, no. September 2019, 2020, doi: 10.1016/j.ijleo.2019.163428.

[8] A. Elhalil *et al.*, "Synthesis, characterization and efficient photocatalytic activity of novel Ca/ZnO-Al2O3 nanomaterial," *Mater. Today Commun.*, vol. 16, pp. 194–203, 2018, doi: 10.1016/j.mtcomm.2018.06.005.

[9] Y. K. Choi, K. M. Kim, Y. Jang, H. Jeong, V. Singh, and S. K. Rangarajulu, "Investigations on the ZnO- and Cr-doped ZnO powders," *Bull. Mater. Sci.*, vol. 42, no. 4, 2019, doi: 10.1007/s12034-019-1832-2.

[10] L. Palanikumar, S. N. Ramasamy, and C. Balachandran, "Size-dependent antimicrobial response of zinc oxide nanoparticles," *IET Nanobiotechnology*, vol. 8, no. 2, pp. 111–117, 2014, doi: 10.1049/iet-nbt.2012.0008.

[11] G. Vijayaprasath *et al.*, "Role of nickel doping on structural, optical, magnetic properties and antibacterial activity of ZnO nanoparticles," *Mater. Res. Bull.*, vol. 76, pp. 48–61, 2016, doi: 10.1016/j.materresbull.2015.11.053.

[12] A. T. Ravichandran and R. Karthick, "Enhanced photoluminescence, structural, morphological and antimicrobial efficacy of Co-doped ZnO nanoparticles prepared by Co-precipitation method," *Results Mater.*, vol. 5, no. January, p. 100072, 2020, doi: 10.1016/j.rinma.2020.100072.

[13] M. P. Dasari, U. Godavarti, and V. Mote, "Structural , morphological , magnetic and electrical properties of Ni-doped ZnO nanoparticles synthesized by co-precipitation method," vol. 3, pp. 100–110, 2018.

[14] S. Roy, M. P. Ghosh, and S. Mukherjee, "Introducing magnetic properties in Fe-doped ZnO nanoparticles," *Appl. Phys. A Mater. Sci. Process.*, vol. 127, no. 6, Jun. 2021, doi: 10.1007/s00339-021-04580-z.

[15] Y. Liu, S. Zhu, Z. Gu, C. Chen, and Y. Zhao, "Toxicity of manufactured nanomaterials," *Particuology*, vol. 69, pp. 31–48, 2022, doi: 10.1016/j.partic.2021.11.007.

[16] M. J. Haque, M. M. Bellah, M. R. Hassan, and S. Rahman, "Synthesis of ZnO nanoparticles by two different methods & comparison of their structural, antibacterial, photocatalytic and optical properties," *Nano Express*, vol. 1, no. 1, 2020, doi: 10.1088/2632-959X/ab7a43.

[17] N. Chauhan, V. Singh, S. Kumar, and R. L. Dhiman, "Influence of Nickel, Silver, and Sulphur Doping on the Photocatalytic Efficiency of Mesoporous ZnO Nanoparticles," *Arab. J. Sci. Eng.*, vol. 45, no. 1, pp. 249–259, 2020, doi: 10.1007/s13369-019-04291-x.

[18] N. Guermat, W. Daranfed, I. Bouchama, and N. Bouarissa, "Investigation of structural, morphological, optical and electrical properties of Co/Ni co-doped ZnO thin films," *J. Mol. Struct.*, vol. 1225, pp. 1–7, 2021, doi: 10.1016/j.molstruc.2020.129134.

[19] A. Paskaleva *et al.*, "Structural, morphological and optical properties of atomic layer deposited transition metal (Co, Ni or Fe)- doped ZnO layers," *J. Mater. Sci. Mater. Electron.*, vol. 32, no. 6, pp. 7162–7175, 2021, doi: 10.1007/s10854-021-05425-4.

[20] H. Pan, Y. Zhang, Y. Hu, and H. Xie, "Effect of cobalt doping on optical, magnetic and photocatalytic properties of ZnO nanoparticles," *Optik (Stuttg).*, vol. 208, no. January, 2020, doi: 10.1016/j.ijleo.2020.164560.

[21] K. Raja, P. S. Ramesh, and D. Geetha, "Synthesis, structural and optical properties of ZnO and Ni-doped ZnO hexagonal nanorods by Co-precipitation method," *Spectrochim. Acta - Part A Mol. Biomol. Spectrosc.*, vol. 120, pp. 19–24, 2014, doi: 10.1016/j.saa.2013.09.103.

[22] S. Debnath and R. Das, "Cobalt doping on nickel ferrite nanocrystals enhances the micro-structural and magnetic properties: Shows a correlation between them," *J. Alloys Compd.*, vol. 852, p. 156884, 2021, doi: 10.1016/j.jallcom.2020.156884.

[23] P. Shunmuga Sundaram, T. Sangeetha, S. Rajakarthihan, R. Vijayalaksmi, A. Elangovan, and G. Arivazhagan, "XRD structural studies on cobalt doped zinc oxide nanoparticles synthesized by coprecipitation method: Williamson-Hall and size-strain plot

approaches," *Phys. B Condens. Matter*, vol. 595, no. July, p. 412342, 2020, doi: 10.1016/j.physb.2020.412342.

[24] P. Shunmuga Sundaram, T. Sangeetha, S. Rajakarthihan, R. Vijayalaksmi, A. Elangovan, and G. Arivazhagan, "XRD structural studies on cobalt doped zinc oxide nanoparticles synthesized by coprecipitation method: Williamson-Hall and size-strain plot approaches," *Phys. B Condens. Matter*, vol. 595, p. 412342, 2020, doi: 10.1016/j.physb.2020.412342.